Quantum dots in microcavities: from single spins to engineered states of light
Steindl, P.

5 Single-photon addition and photon correlations

Non-Gaussian multi-photon states of light including displaced Fock states and single-photon-added coherent states are key for continuous-variable quantum information processing. Traditionally, these states are produced using heralded single-photon sources based on nonlinear optics, which relatively easily allows matching of the temporal-spectral properties of the single photon and the coherent state; but this method is intrinsically non-deterministic. Here we theoretically study single-photon addition using different sources of single photons including near-deterministic sources based on quantum dots, and investigate the influence of single-photon purity, brightness, and indistinguishability. We derive analytical results and find that the two-photon correlation function of the generated quantum light can be used to robustly characterize and optimize the fidelity of the generated states.

5.1 Introduction

In order to implement classically hard-to-simulate continuous variable (CV) photonic quantum circuits [175], Wigner negative [176, 177] resources such as non-Gaussian input states are necessary. These states are also interesting in other fields, for instance they promise improved security in quantum key distribution [178–181], and might find use in quantum metrology [62]. Despite several classes of non-Gaussian states have been identified over the past two decades [182–184], they remain notoriously challenging to produce [185]. The manipulation of light fields on the single-photon level using photon subtraction [186] or addition [187–189] allows for flexible engineering of the photon number statistics [85, 190–192], these operations are the experimental analogues of the application of the annihilation and creation operators a and $a^\dagger$ on a well-defined optical mode [193].

Single-photon addition can be realized by emission of one photon of a photon pair into the classical input light field in a nonlinear crystal [187–189], using a three-level quantum system in an optical cavity [194, 195] or by interference of the input light (e.g. coherent light) with a single photon on an (unbalanced) beam splitter [196–199]. In all cases, the addition of the single photon alters the photon statistics of the input light dramatically [200] resulting in genuinely non-classical states of light [201] for both coherent light [202] or thermal light [203] used as the input.

In contrast to single-photon addition, the related process of single-photon subtraction produces non-classical non-Gaussian states only if performed on a non-classical input state [184, 204]. Single-photon subtraction can be realized in the simplest case using post-selection on single-photon detection at a beam splitter [186, 205].

To date, photon addition was realized mostly using heralded single-photon sources [206, 207] based on spontaneous parametric down-conversion (SPDC). Because the number of photon pairs produced by SPDC follows a thermal distribution [208, 209], heralded production of single photons suffers from a trade-off between single-photon brightness and purity, only recently extensive efforts have improved this to some extend [209, 210]. At the same time, there is fast progress with true single-photon sources (SPSs) [211] based on III-V semiconductor quantum dots in optical microcavities that would in-principle enable fully deterministic and pure single-photon production [13, 15, 17, 18, 28, 57, 102, 103], and with this also deterministic single-photon addition. Here, we investigate and compare single-photon addition for different photon sources including the effect of brightness, purity and indistinguishability. We calculate the second-order correlation function of the resulting quantum light, and find that photon correlation measurement of displaced Fock states is a robust method to optimize wave-function overlap such as mode-matching on the beam splitter.

5.2 Displaced Fock states from quantum interference

A non-polarizing beam splitter (BS) enables quantum interference of two incident optical fields. Based on the beam splitter input-output relations [208, 212], more complex photonic states can be synthesized, the prime example is the Hong-Ou-Mandel (HOM) effect, where two identical single photons "bunch" at the beam splitter [27]. This effect is used for the characterization of the photon indistinguishability of single-photon sources [28], to entangle photons [5, 213], prepare photon-number superposition [85, 214], and in boson sampling [215]. A beam splitter also enables implementing the displacement operator by mixing the input state with a strong coherent state [216]. This effect lies at the heart of

homodyne detection and also allows for state Wigner function tomography [185]. All these effects originate from quantum-state manipulation by interference at the beam splitter.
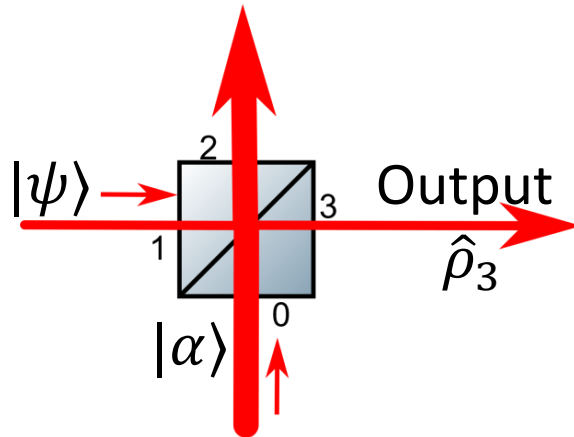

Figure 5.1: General scheme: In a possibly unbalanced beam splitter, the input state $|\psi\rangle$, e.g. a single-photon state, and a classical state of light, for instance the coherent state $|\alpha\rangle$, undergo quantum interference, resulting in possibly non-Gaussian output light.

We assume a loss-less low-reflectivity beam splitter ($R \ll 1$) sketched in Fig. 5.1 and study quantum interference of a coherent state $|\alpha\rangle$ and a state of the form $|\psi\rangle = \sqrt{p_0}|0\rangle + \sqrt{p_1}|1\rangle + \sqrt{p_2}|2\rangle$ by observing output mode 3, ignoring output mode 2. This situation is closely related but different from the conditional generation of single-photon added coherent states using heralding on zero [196, 197] or single-photon detection [217, 218] in mode 2. Our protocol does not rely on heralding and our form of $|\psi\rangle$ allows investigation of the relevant single-photon source properties, the single-photon brightness p_1 and purity $1 - p_2$. The structure of $|\psi\rangle$ has been chosen with the ambition to be able to compare SPDC-based sources (where $p_1 \ll 1$, $p_0 \approx 1 - p_1$, and $p_2 = p_1^2$ in the low-gain limit) and true single-photon sources with $p_1 \approx 1$ and $p_0, p_2 \approx 0$ [219].

Assuming for now that $|\alpha\rangle$ and $|\psi\rangle$ are perfectly indistinguishable in all degrees of freedom, we can calculate the quantum state emerging from the beam splitter in the low-reflection approximation and obtain [199, 216, 220]

$$|\psi_{\text{out}}\rangle \approx \sqrt{p_0}|\gamma\rangle_2|\beta\rangle_3 + \sqrt{p_1}\left(ir\hat{D}_2(\gamma)|1\rangle_2|\beta\rangle_3 + t\hat{D}_3(\beta)|\gamma\rangle_2|1\rangle_3\right)$$
$$+ \sqrt{p_2}\left(\sqrt{2}irt\hat{D}_2(\gamma)\hat{D}_3(\beta)|1\rangle_2|1\rangle_3 + t^2\hat{D}_3(\beta)|\gamma\rangle_2|2\rangle_3 - r^2\hat{D}_2(\gamma)|2\rangle_2|\beta\rangle_3\right).$$

Here, $\hat{D}_x(\gamma) = e^{\gamma x^\dagger - \gamma^* x}$ is the displacement operator operating on mode x, and $\alpha = \gamma/t = -i\beta/r$.

We are only interested in the output mode 3, therefore we trace out mode 2 leading to (from now on, the subscript 3 is dropped)

$$\hat{\rho}_3 = \hat{D}(\beta)\left[A_0|0\rangle\langle0| + A_1|1\rangle\langle1| + A_2|2\rangle\langle2|\right]\hat{D}(\beta). \tag{5.1}$$

The result is a mixture of displaced vacuum, single- and two-photon states, with the mixing probabilities $A_0 = p_0 + p_1 R + p_2 R^2$, $A_1 = Tp_1 + 2RTp_2$, and $A_2 = T^2 p_2$. The mixing probabilities and displacement depend on the beam splitter reflectivity R and transmissivity T, which can be used to control the final state, next to changing the input state $|\psi\rangle$. Eq. (5.1) reduces to results of Windhager et al. [221] in the weak single-photon limit, $p_2 = 0$.

5.2.1 Influence of loss

To give a fair comparison between heralded and true single-photon sources, we implement photon loss in the optical channels. Because coherent states $|\alpha\rangle$, eigenstates of the annihilation operator, do not change their character under loss [222, 223], we model loss only in the $|\psi\rangle$ channel by an additional beam splitter of transmission η. Similar to above, we calculate the final state in mode 3 including photon loss. As expected, the structure of the state in Eq. (5.1) is not altered, only the mixing probabilities A_i are changed and now scale with $\tilde{p}_i$ instead of p_i: $\tilde{p}_0 = \sum_{j=0}^{2} [(1-\eta)^{j-1} p_j]$, $\tilde{p}_1 = \eta(p_1 + 2p_2 - 2\eta p_2)$, and $\tilde{p}_2 = \eta^2 p_2$.

5.3 Photon correlations

In experiments, the 2nd-order intensity or photon correlation function $g^{(2)}(\tau)$ is easily accessible because the required Hanbury-Brown & Twiss (HBT) setup [224] is simple, and since it is insensitive to detection efficiencies and loss; further it can be extended to higher-order photon correlations [225]. We can calculate the zero-delay correlation
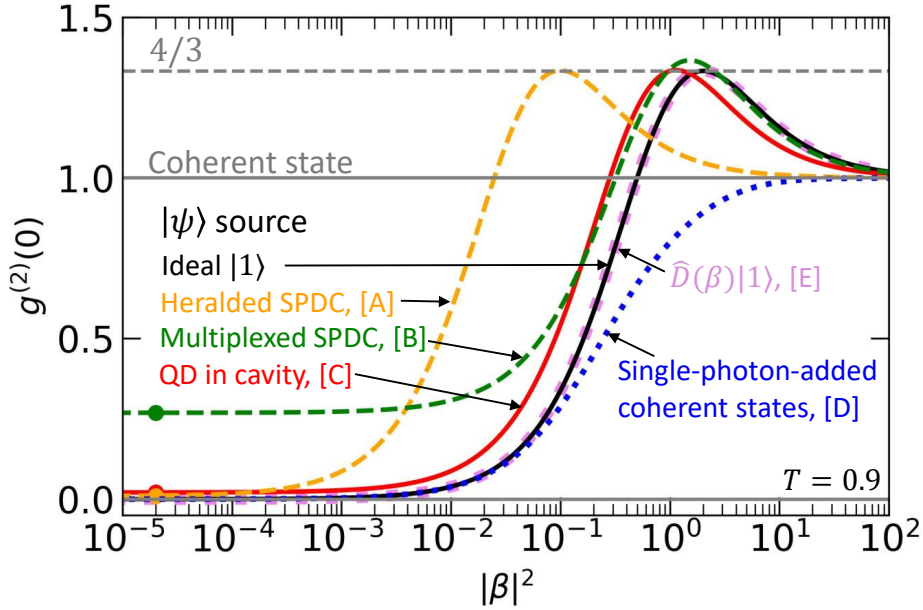

Figure 5.2: Comparison of $g^{(2)}(0)$ as a function of the reflected coherent state $|\beta|^2$ for photon addition at a beam splitter with transmission $T = 0.9$ by quantum interference of $|\alpha\rangle$ with $|\psi\rangle$ for different sources for $|\psi\rangle$: Heralded SPDC single-photon source (orange, A [207]), multiplexed SPDC source (green, B [209]), QD-based true single-photon source (red, C [15]) and an ideal single-photon Fock state (black). We also show $g^{(2)}(0)$ for the single-photon added coherent state (blue, D [187]) and for a displaced single photon state (purple, E [226]). Symbols represent experimentally reported $g^{(2)}(0)$.

function $g^{(2)}(0)$ from the state $\hat{\rho}_3$ using commutation relations between displacement and ladder operators [208, 227], after some steps shown in Appendix 5.7.1 we obtain

$$g^{(2)}(0) = \frac{|\beta|^4 + 4|\beta|^2 T\eta(p_1 + 2p_2) + 2T^2\eta^2 p_2}{[|\beta|^2 + T\eta(p_1 + 2p_2)]^2}.$$
(5.2)

This expression is directly dependent on the photon statistics of $|\psi\rangle$ and allows easy comparison of $g^{(2)}(0)$ for various photon emitters as shown in Fig. 5.2, as a function of the strength of the reflected coherent state $|\beta|^2 = R|\alpha|^2$. In general, we observe a gradual transition from the correlation function of the input state $|\psi\rangle$ $[g^{(2)}_{|\psi\rangle}(0)]$ to that of the coherent state $[g^{(2)}_{|\alpha\rangle}(0) = 1]$ with increasing coherent state strength.

First, we assume a negligible multi-photon contribution in $|\psi\rangle$, which is a good approximation of current QD-based and weak heralded SPSs with purity exceeding 0.98. Under this condition, $g^{(2)}(0)$ reduces to the expression reported and experimentally confirmed by Shen et al. [228] with the (detected) single-photon brightness $\tilde{p}_1 = \eta p_1$:

$$g^{(2)}(0) = \frac{|\beta|^4 + 4|\beta|^2 T\tilde{p}_1}{[|\beta|^2 + T\tilde{p}_1]^2}. \tag{5.3}$$

Interestingly, this function has a global maximum of 4/3 in the parameter space of $\{T, \tilde{p}_1, |\alpha|^2\}$ connecting all experimental parameters defining the problem, i.e., the splitting ratio of the BS, the strength of the coherent state given by its mean photon number $|\alpha|^2$, and the single-photon source brightness $\tilde{p}_1$ by $R|\alpha|^2 = 2\tilde{p}_1 T$.

Now, we focus on the evolution of the quantum state $\hat{\rho}_3$ prepared with an ideal single-photon state ($|\psi\rangle = |1\rangle$) while the coherent state strength gradually increases from zero. On top of the naturally expected quantum-to-classical state transition from the initially purely quantum state (the single-photon Fock state with $g^{(2)}_{|1\rangle}(0) = 0$) into a classical coherent state (with $g^{(2)}_{|\alpha\rangle}(0) = 1$), the theory also predicts a regime of photon bunching with $g^{(2)}(0) > 1$ with a maximal $g^{(2)}(0)$ of 4/3. As expected, the photon correlation function converges to $g^{(2)}_{\hat{D}(\beta)|1\rangle}(0)$ for $T \to 1$ and $\tilde{p}_1 = 1$ as theoretically predicted for a pure displaced Fock state $g^{(2)}_{\hat{D}(\beta)|1\rangle}(0) = \frac{|\beta|^2(4+|\beta|^2)}{(1+|\beta|^2)^2}$ [226].

In Fig. 5.2, we compare $g^{(2)}(0)$ achieved with several experimentally available single-photon sources, and in Table 5.1, we show the relevant characteristics of these sources. For example, heralded SPDC sources with a high single-photon purity $g^{(2)}_{|\psi\rangle}(0) \approx 2\tilde{p}_2/\tilde{p}_1^2 \approx 0.01$ are typically operated in low photon number regime (mean photon number ~ 0.05) to minimize multi-photon contributions; which also results in the limited brightness $\tilde{p}_1 \approx 0.05$ [207]. As expected from Eq. (5.3), we observe the reduction in $\tilde{p}_1$ as a shift towards weaker coherent state strength for which $g^{(2)}(0)$ becomes maximal. The brightness $\tilde{p}_1$ of a heralded SPDC source can be artificially increased beyond the thermal statistics limit by time or spatial-bin multiplexing [229]. For example, Kaneda et al. [209] achieved $\tilde{p}_1 = 0.667$ by multiplexing 40 time bins at the cost of worsen single-photon purity to $g^{(2)}_{|\psi\rangle}(0) \approx 0.269$. For the parameters reported in Ref. [209] we find (i) a shift of the bunching regime towards higher $|\beta|^2$ due to higher $\tilde{p}_1$, and (ii) $g^{(2)}(0)$ exceeding slightly 4/3 (by ≈ 0.03) due to non-negligible multi-photon contributions in $|\psi\rangle$.

In contrast to SPDC sources, the single-photon purity of QD-based single-photon sources is, in principle, independent of the brightness. However, the purity can be compromised by QD re-excitation [230, 231] and/or non-ideal excitation-laser filtering [54, 101], contaminating the single photons with multi-photon components. Nevertheless, the purity often exceeds 0.98. Therefore, it is not surprising to expect with the best available QD-based sources [15] similar behavior of $g^{(2)}(0)$ as obtained for an ideal single-photon Fock state, again with its maximal value of 4/3, at $|\beta|^2 = 2T\tilde{p}_1 = 1.026$.

Finally, we compare the photon correlations of $\hat{\rho}_3$ with correlations expected for theoretical single-photon-added coherent states $Ca^\dagger|\beta\rangle$ with $C = 1/\sqrt{1 + |\beta|^2}$ [187], which

	Heralded SPDC [207]	Multiplexed SPDC [209]	Quantum dot [15]
Purity $g^{(2)}_{|\psi\rangle}(0)$	0.01	0.269	0.021
Brightness $\tilde{p}_1$	0.045	0.667	0.566
$\tilde{p}_0$	0.953	0.231	0.43
$\tilde{p}_2$	0.002	0.102	0.003

Table 5.1: Single-photon purity, brightness (and $\tilde{p}_0$ and $\tilde{p}_2$) of several single photon sources used for the evaluation of $g^{(2)}(0)$ in Fig. 5.2.

can be easily calculated: $g^{(2)}_{Ca^\dagger|\beta\rangle}(0) = \frac{4|\beta|^2 + 5|\beta|^4 + |\beta|^6}{|1 + 3|\beta|^2 + |\beta|^4|^2}(1 + |\beta|^2)$. Notably, $g^{(2)}_{Ca^\dagger|\beta\rangle}(0)$ shows a monotonous transition from single-photon to coherent-state correlations without a region of photon bunching. This absence can be used for discriminating single-photon added coherent states from displaced Fock states, which are hard to distinguish otherwise [232].

5.4 Effect of photon indistinguishability

Up to now, we have assumed perfect indistinguishability, or wave-function overlap, of the interfering light fields, now we discuss fields with reduced overlap. First, we introduce an extra degree of freedom enabling us to define indistinguishability - we choose polarization for simplicity, where for linearly polarized input fields, the indistinguishability can easily be modified by polarization rotation with a half-waveplate (HWP). We introduce a HWP in the beam splitter input channel 0 and vary its polarization by adjusting the HWP angle $\theta/2$, as sketched in the inset of Fig. 5.3. For example, an incident H-polarized coherent state $|\alpha, 0\rangle$ is transformed by the HWP to $|\alpha\cos\theta, \alpha\sin\theta\rangle$; we use the two-entry ket notation representing H and V polarization, which allows full control over the mutual indistinguishability M between the input fields. The beam splitter transformation and final states are shown in Appendix 5.7.1, we obtain

$$g^{(2)}_\theta(0) = \frac{|\beta|^4 + 2|\beta|^2 T\eta(1 + M)(p_1 + 2p_2) + 2T^2\eta^2 p_2}{[|\beta|^2 + T\eta(p_1 + 2p_2)]^2} .$$

In Fig. 5.3, these photon correlations are shown for varied indistinguishability. If the photons are maximally indistinguishable ($M = \cos^2\theta = 1$), the model reduces to Eq. (5.2) and a prominent bunching region appears, which is absent for the fully distinguishable case with $M = 0$.

The strong dependency of the correlation function caused by the high sensitivity of multi-photon interference on the indistinguishability [233] is a remarkable quality enabling fidelity optimization of the prepared state. Moreover, the correlation measurement performed in the HBT interferometer is loss and imperfect-detection tolerant, in contrast to homodyne Wigner tomography requiring above 50% detection efficiency to successfully reconstruct Wigner negativity [234] and another phase-stabilized coherent state acting as the local oscillator. The combination of these facts makes the correlation-function method experimentally feasible for optimizing indistinguishability and mode-matching at the beam splitter.
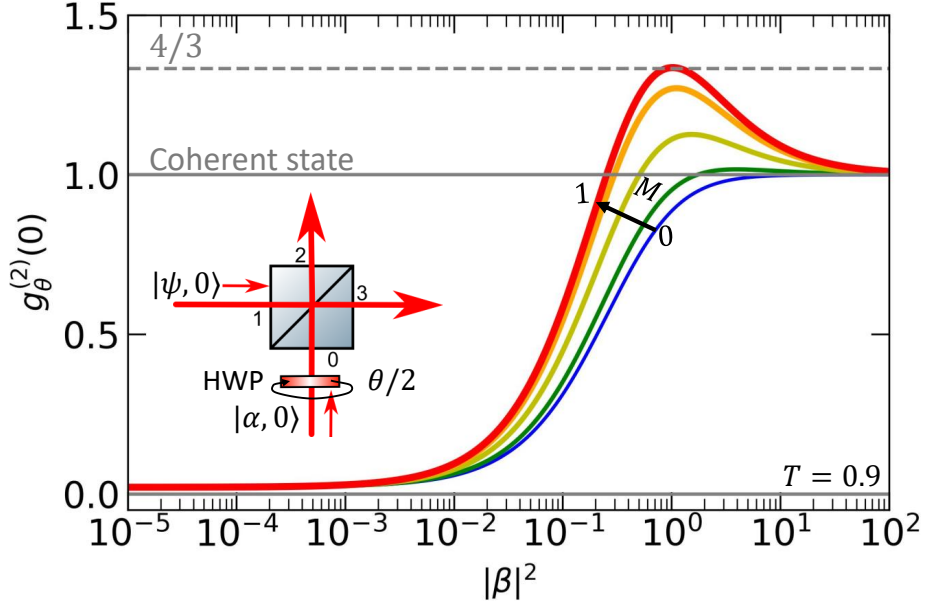
Figure 5.3: The effect of photon indistinguishability on displaced Fock states. The plot shows $g_\theta^{(2)}(0)$ as a function of the coherent-state brightness for different indistinguishability M between the coherent state and single photons produced by a quantum dot - cavity single photon source [15]. M is changed by rotating the polarization of one of the beam splitter inputs with a half-wave plate.

Despite the simplicity of the technique, achieving true indistinguishability and thus observation of a 4/3 photon bunching requires fine optimization. To date, the maximal experimentally reported value is ~ 1.26 of Shen et al. [228], where the indistinguishability is limited to 0.86 by a non-ideal spectral-temporal overlap of the coherent state from attenuated laser pulses and heralded single photons.

5.5 Single-photon addition with quantum dot sources

Figure 5.4 shows an experimental setup for single-photon addition on a beam splitter: the coherent states are made by an attenuated laser, and a QD integrated into an optical microcavity operated at cryogenic temperatures is used as a single-photon source (SPS). For the generation of displaced Fock states, a single-mode fiber splitter is used instead of a free-space beam splitter. The fiber optic splitter (ration R:T=10:90) enables (i) long-term stable spatial mode overlap between the input fields and (ii) flexible connectivity to fiber-based optical networks for possible applications.

First, we concentrate on the generation of single photons. The QD on-resonance with the optical cavity is excited with a few-10 picosecond long laser pulse. The pulse duration needs to be optimized to minimize QD re-excitation [230, 231] either by fast electro-optic modulation (EOM) of narrow-bandwidth continuous-wave laser (cw laser 1) [235] or using ultra-short duration pulsed laser together with grating-based pulse shaping [236]. The excitation polarization and laser power are chosen to reach the maximal QD population inversion, leading to maximal single-photon brightness p_1 [237]. Then, the emitted single photons are separated from the excitation laser and collected in a single-mode fiber attached to the fiber splitter. Depending on the excitation scheme, the reflected resonant

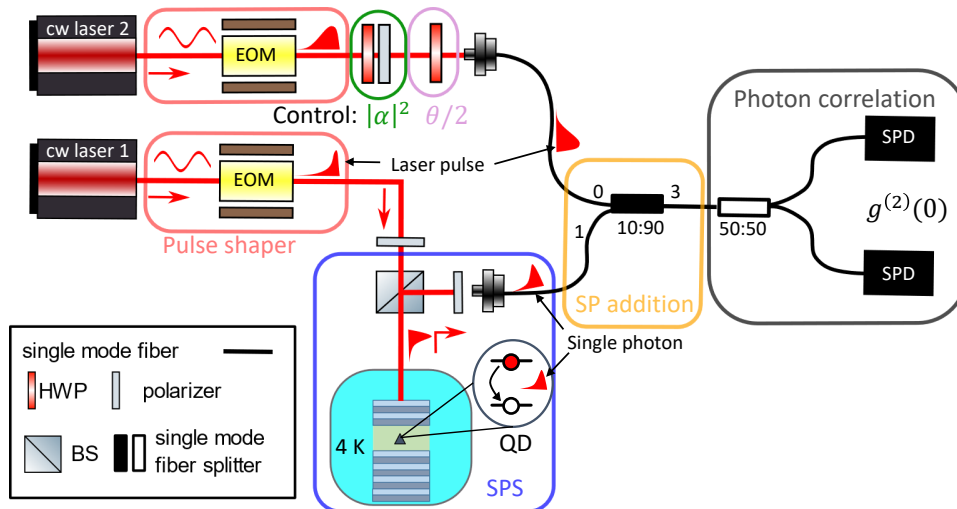(non-resonant) laser light is filtered out using cross-polarization [54, 101], or spectral [17] filtering.

Figure 5.4: Experimental setup for single-photon addition with a QD-based single-photon source. A few-picosecond long laser pulse excites the QD-cavity device, spontaneously emitting a single photon upon relaxation. The single photon is separated from reflected laser light, collected in a polarization-maintaining fiber, and interfered with a coherent state from another laser source with control over all degrees of freedom on a polarization-maintaining fiber splitter.

Now, we discuss the preparation of coherent states $|\alpha\rangle$. Laser 2 is tuned to be resonant with the QD emission and the strength $|\alpha|^2$ of the coherent state can be tuned with by a half-wave plate (HWP) in combination with a linear polarizer before being coupled into a single-mode fiber connected to the fiber splitter (input port 0). To achieve maximal state overlap on the fiber splitter, we prepare the coherent states in the form of optical pulses. This, in contrast to the continuous-wave regime, enables us to control all degrees of freedom of the coherent state and engineer them for maximal interference with the single photons: (i) the spatial degrees are matched using a single-mode fiber splitter, (ii) the polarization of the coherent state is controlled by adjusting the angle $\theta/2$ of an extra half-wave plate placed in front of the fiber coupler, and finally (iii), the arrival time synchronization and spectral-temporal overlap can be optimized by pulse shaping of the coherent laser pulses. For example, perfect matching to the lifetime-limited trion emission with mono-exponential decay described by the trion lifetime T_1 [238] requires exponential coherent state pulses with duration T_1.

This wave-function overlap optimization, requiring iterative fine-tuning of all modes of the light fields, becomes very challenging experimentally in the presence of photon loss and limited detection efficiencies. However, as also discussed above, the wave-function overlap can be maximized based on the photon-correlation $g^{(2)}(0)$ signal, which is insensitive to experimental imperfections.

Finally, we comment on the displaced Fock state generation rates achievable with current QD-based single-photon source technology. The rate is, in principle, limited only by the emission properties of the QD, i.e., its in-fiber brightness defining single-photon gain per pulse and T_1 limiting the excitation rate. In-fiber single-photon rates up to $1\,\mathrm{GHz}$ with an in-fiber brightness of $\tilde{p}_1 = 0.57$ at a lifetime of $T_1 \sim 50\,\mathrm{ps}$ has been obtained [15].

In comparison, all currently available SPDC-based sources have more than one order of magnitude smaller single-photon rates due to heralding and necessary low $\tilde{p}_1$, or limited multiplexing rates, a comparison is given in Ref. [209].

5.6 Conclusions

In conclusion, we have theoretically studied the second-order photon correlation function $g^{(2)}(0)$ of displaced Fock states generated by quantum interference of coherent and single-photon states. We have modelled the single photons to account for experimentally unavoidable imperfections, limited brightness and reduced purity, and have derived formulas directly connecting the resulting photon correlations to the single-photon source properties. We have shown that for the case of true single-photon sources, the correlations show universal photon bunching with $g^{(2)}(0)$ reaching 4/3. This bunching is very sensitive to the indistinguishability of the single photons and the coherent state at the beam splitter, which can therefore be used for optimization of indistinguishability at the beam splitter including mode-matching and single-photon properties, and allows discrimination of single-photon added coherent states and displaced Fock states. Finally, we have evaluated an experiment with a realistic quantum-dot based true single-photon source, which will allows production of GHz-rate displaced Fock states that might be useful for quantum key distribution [178–181] and photon boson sampling [232, 239].

5.7 Appendix

5.7.1 Derivation of $g_\theta^{(2)}(0)$

Here we discuss essential steps in the derivation of $g_\theta^{(2)}(0)$ presented in the main text. As shows in Fig. 5.3, the HWP enables continuous variation of the polarization by adjusting its angle $\theta/2$. We use two-component ket notation to represent the HWP transformation; the initially H-polarized coherent state is transformed as $|\alpha, 0\rangle \xrightarrow{\text{HWP}(\theta/2)} |\alpha \cos\theta, \alpha \sin\theta\rangle$. Under this transformation in the low-reflection approximation, the state emerging from the BS in mode 3 after a partial trace over mode 2 is

$$\hat{\rho}_3 = \hat{D}_V(\beta_V)\hat{D}_H(\beta_H)\left[A_0|0,0\rangle\langle 0,0| + A_1|1,0\rangle\langle 0,1| + A_2|2,0\rangle\langle 0,2|\right]\hat{D}_H^\dagger(\beta_H)\hat{D}_V^\dagger(\beta_V).$$

This state is a two-mode mixture of displaced Fock states with displacement $\beta_V = \beta\sin\theta$, $\beta_H = \beta\cos\theta$. The second-order photon correlation function can be calculated from $g_\theta^{(2)}(0) = \frac{\text{Tr}(\hat{\rho}_3 a^\dagger a^\dagger aa)}{|\text{Tr}(\hat{\rho}_3 a^\dagger a)|^2}$. In the following derivation, we have used: (i) the cyclic properties of the trace, (ii) the commutation relations between ladder and displacement operators [227], (iii) unitarity of the displacement operator, and (iv) the relation $\hat{n} = \hat{n}_H + \hat{n}_V$ connecting the polarization modes to non-polarized detection. For simplification, we define $\hat{\rho}_{3,H} = A_0|0\rangle\langle 0| + A_1|1\rangle\langle 1| + A_2|2\rangle\langle 2|$, and evaluate the numerator and denominator separately.

The numerator:

$$\text{Tr}_{V,H}[\hat{\rho}_3 a_H^\dagger a_H] = \text{Tr}_H[(a_H^\dagger + \beta_H^*)(a_H + \beta_H)\hat{\rho}_{3,H}] = A_1 + 2A_2 + |\beta_H|^2$$
$$\text{Tr}_{V,H}[\hat{\rho}_3 a_V^\dagger a_V] = \text{Tr}_{H,V}[(a_V^\dagger + \beta_V^*)(a_V + \beta_V)\hat{\rho}_{3,H}] = |\beta_V|^2$$
$$\text{Tr}_{V,H}(\hat{\rho}_3 a^\dagger a) = \text{Tr}_{V,H}[\hat{\rho}_3(a_H^\dagger a_H + a_V^\dagger a_V)] = A_1 + 2A_2 + |\beta|^2$$

The denominator:

$$\text{Tr}_{V,H}[\hat{\rho}_3 \hat{n}_H^2] = \text{Tr}_H\{[(a_H^\dagger + \beta_H^*)(a_H + \beta_H)]^2\hat{\rho}_{3,H}\} = \text{Tr}_H\{[(a_H^\dagger + \beta_H^*)(a_H + \beta_H)]^2\hat{\rho}_{3,H}\}$$
$$= \text{Tr}_H[(\hat{n}_H^2 + 4|\beta_H|^2\hat{n}_H + |\beta_H|^2 + |\beta_H|^4)\hat{\rho}_{3,H}]$$
$$= A_1 + 4A_2 + 4|\beta_H|^2(A_1 + 2A_2) + |\beta_H|^2 + |\beta_H|^4$$
$$\text{Tr}_{V,H}[\hat{\rho}_3 \hat{n}_V^2] = \text{Tr}_H\{[(a_V^\dagger + \beta_V^*)(a_V + \beta_V)]^2\hat{\rho}_{3,H}\} = |\beta_V|^2 + |\beta_V|^4$$
$$\text{Tr}_{V,H}[\hat{\rho}_3 \hat{n}_H \hat{n}_V] = |\beta_V|^2\text{Tr}_H\{(a_H^\dagger + \beta_H^*)(a_H + \beta_H)\hat{\rho}_{3,H}\} = |\beta_V|^2(A_1 + 2A_2 + |\beta_H|^2)$$
$$\text{Tr}_{V,H}(\hat{\rho}_3 a^\dagger a^\dagger aa) = \text{Tr}_{V,H}[\hat{\rho}_3(\hat{n}_H^2 + 2\hat{n}_H\hat{n}_V + \hat{n}_V^2 - \hat{n}_H - \hat{n}_V)]$$
$$= |\beta|^4 + 2|\beta|^2[1 + \cos^2\theta](A_1 + 2A_2) + 2A_2$$

With this, the photon correlations can be expressed as

$$g_\theta^{(2)}(0) = \frac{|\beta|^4 + 2|\beta|^2[1 + \cos^2\theta](A_1 + 2A_2) + 2A_2}{[|\beta|^2 + A_1 + 2A_2]^2}$$
$$= \frac{|\beta|^4 + 2|\beta|^2 T\eta(1 + \cos^2\theta)(p_1 + 2p_2) + 2T^2\eta^2 p_2}{[|\beta|^2 + T\eta(p_1 + 2p_2)]^2} \quad (5.4)$$

where the correlations in the last step are represented directly in terms of the photon number probabilities of the single-photon source. For the case of fully indistinguishable photonic fields, this reduces to

$$g^{(2)}(0) = \frac{|\beta|^4 + |\beta|^2 T\eta(p_1 + 2p_2) + 2T^2\eta^2 p_2}{[|\beta|^2 + T\eta(p_1 + 2p_2)]^2}. \quad (5.5)$$

This function is maximized for $|\beta|^2 = 2T\eta[p_1 + 2p_2 - p_2/(p_1 + 2p_2)]$. Assuming negligible multi-photon contributions (simply by setting $p_2 = 0$) which is a good approximation of state of the art single-photon sources, the expression in Eq. (5.5) can be further simplified to

$$g^{(2)}(0) = \frac{|\beta|^4 + 4|\beta|^2 T\tilde{p}_1}{[|\beta|^2 + T\tilde{p}_1]^2}$$

where we used the definition of detected single-photon brightness $\tilde{p}_1 = \eta p_1$. Interestingly, this function has a global maximum of $4/3$.

5.7.2 Photon correlations: single-photon-added coherent states vs displaced Fock states

Shen et al. [228] studied photon correlations before, in a notation consistent with our work they have obtained

$$g^{(2)}(0) = \frac{|\beta|^4 + 4|\beta|^2 T\tilde{p}_1 + 4\tilde{p}_1 T|\beta|^4 + \tilde{p}_1 T|\beta|^6}{[\tilde{p}_1 T + |\beta|^2 + 2\tilde{p}_1 T|\beta|^2 + \tilde{p}_1 T|\beta|^4]^2}(1 + \tilde{p}_1 T|\beta|^2).$$

This formula, appearing also in other works [240], is based on a somewhat unconventional ordering of non-commuting operators after the beam splitter transformation, which is inconsistent with literature (e.g. [199, 217, 241, 242]). Nevertheless, for a weak attenuated laser with $|\beta|^2 \ll 1$ and a weak heralded single-photon source ($\tilde{p}_1 \ll 1$) results in the approximate expression

$$g^{(2)}(0) = \frac{|\beta|^4 + 4|\beta|^2 T\tilde{p}_1}{[\tilde{p}_1 T + |\beta|^2]^2},$$

which described well experimental data. Our formalism results in the same result for $p_2 = 0$ and the same approximations. This agreement is not surprising, since the difference arises only from the commutation relation $[\hat{a}, \hat{D}(\beta)] = \beta\hat{D}(\beta)$ [227] which vanishes for weak coherent states.